SCIENCE CHINA
Information Sciences

• RESEARCH PAPER •
Special Focus on Two-Dimensional Materials and Device Applications

April 2021, Vol. 64 140405:1–140405:8
https://doi.org/10.1007/s11432-020-3149-2

Optical emission enhancement of bent InSe thin films

Jiahao XIE & Lijun ZHANG*

State Key Laboratory of Integrated Optoelectronics, Key Laboratory of Automobile Materials of MOE, School of Materials Science and Engineering, Jilin University, Changchun 130012, *China*

Received 13 November 2020/Revised 21 December 2020/Accepted 25 December 2020/Published online 8 March 2021

Abstract In contrast to the majority of two-dimensional semiconductors such as transition metal dichalcogenides, indium selenide (InSe) possesses an intrinsic large out-of-plane oriented band-edge luminescent dipole. This unique anisotropic feature of band-edge optical emissions can be exploited to achieve enhanced optical signal in bent regions of materials created by geometrical modification. We herein investigate based on first-principle calculations the mechanism of this optical emission enhancement by modelling the photoluminescence processes in bent and flat regions of the InSe thin film. We propose in our model that the shorter-wavelength interband transition, labelled as transition B', between the second-highest valence band and the bottom of conduction band plays an important role in the enhancing process. Our model robustly describes the dependence of optical emission enhancement in the bent InSe thin films on thickness, incident light orientation, and excitation photon energy. In particular, we found that when excitation photon energy is lower than the energy of transition B', strong enhancement up to hundreds of times can be obtained by applying an incident light at an angle less than 70° to the InSe layers. Our results provide useful references for modulating luminescent properties of InSe films toward flexible optoelectronic device applications.

Keywords InSe, enhanced luminescence, 2D semiconductor, optical transition, optical anisotropy

Citation Xie J H, Zhang L J. Optical emission enhancement of bent InSe thin films. Sci China Inf Sci, 2021, 64(4): 140405, https://doi.org/10.1007/s11432-020-3149-2

1 Introduction

Two-dimensional (2D) atomically thin van der Waals (vdW) semiconductors exhibit many unique properties, including highly tunable electronic structures and optical properties, large mechanical flexibility, and high carrier mobility, making them excellent candidates for nanoscale electronics and optoelectronics [1–12]. Among the vast family of 2D materials, InSe has emerged as a promising 2D semiconductor material in recent years [13–24]. Owing to the combined effect of quantum confinement and interlayer coupling [13, 25–29], the bandgap of InSe is highly tunable, ranging from about 1.25 eV for bulk crystal [30] to 2.1 eV for monolayer (ML) InSe [14], covering the near-infrared to yellow visible light region. InSe features a unique electronic structure. The conduction band (CB) mainly consists of dispersive antibonding In-s states, leading to a small effective mass of CB and a room temperature carrier mobility up to 10^3 cm^2V^{-1}, which is the highest among all 2D vdW materials [15]. However, the top valence band (VB) mainly consists of Se-p_z orbitals, resulting in a small transition dipole moment (TDM) of the band edge optical transition for light polarized along the in-plane directions, and a large TDM for light polarized along the out-of-plane direction, in contrast to the case of transition metal dichalcogenides (TMDCs) [14–16, 31–33]. The bandgap of InSe experiences a direct-to-indirect transition as the thickness decreasing from bulk to few layers [34]. The unique electronic structure leads to weak optical emissions in few-layers InSe, especially in the bilayer and ML InSe [13–15], limiting their potential application in optoelectronics. Many efforts have been spent on tuning and enhancing the optical emissions of few-layers InSe. It has been demonstrated that external strain can effectively tune the electronic structure and wavelength of optical emissions of few-layers InSe [19, 35]. However, there is no evidence that strain can induce carrier localization to enhance the optical emission intensity of InSe. The anisotropy of optical

* Corresponding author (email: lijun_zhang@jlu.edu.cn)

© Science China Press and Springer-Verlag GmbH Germany, part of Springer Nature 2021

transitions of InSe has a significant influence on its optical emission. The angle-dependent photoluminescence (PL) results show that enhanced PL intensity can be obtained along non-vertical directions to the InSe plane [31, 34, 36]. Geometrical modification of InSe films can produce bent regions on the InSe plane and become an effective way to enhance the optical emission of InSe utilizing the anisotropy of its optical transitions. In the bent regions, InSe surface will interact non-vertically with the incident and emissive lights, and more optical transitions can be excited, leading to enhanced optical emission in the bent regions. Brotons-Gisbert et al. [14] placed exfoliated InSe sheets onto aggregates of SiO2 nanoparticles and obtained enhanced optical emission in the textured region. Li et al. [32] put the InSe flake onto Si/SiO2 substrate to form ridge regions and achieved enhanced light emission in the ridge region. Mazumder et al. [16] obtained reproducible bent InSe shapes with enhanced optical emission by fabricating InSe flakes onto Si substrate with periodic Si-pillars. The last work demonstrated that the optical emission enhancement of bent InSe flakes arises from exploiting the anisotropy of InSe's optical transitions, by a combined experiment and theoretical calculation approach.

Though it is proved that the anisotropy of the optical transitions can be used to enhance the optical emission of InSe thin films, there still lacks a thorough understanding of the enhancing process and the involved optical transitions. Two optical transitions are considered significant in previous studies. One is the band edge transition, labelled as transition A, which is mainly allowed for light polarized along out-of-plane direction. Another one, labelled as transition B, is the interband transition between the bottom of CB and the deeper VB dominated by Se-p_{xy} orbitals, thus fully allowed for light polarized along in-plane directions. In a recent experiment work [16], a trend of the emission enhancement in the bent regions of InSe thin films depending on film thickness is revealed, without the excitation of transition B. This result implies that the optical transitions with energy between transitions A and B also influence the enhancing process. To gain more understanding of the mechanism of optical emission enhancement from bent InSe thin film, in this work, we present a systematic research of the PL processes in bent and flat regions of InSe film, based on first-principle calculations. This work consists of three parts. First, we present a detailed analysis of the optical transitions of few-layers InSe. Second, we build an analytical model of the PL process in bent and flat regions of InSe film, to simulate the optical emission enhancement as a function of the incident angle and photon energy of the excitation light. Finally, we calculate the absorption coefficients of 1–9 layers InSe and get the numerical solution of the emission enhancement model. We find that the interband optical transition, labelled as transition B', between the second-highest VB and the bottom of CB, is important while exploiting the anisotropy of optical transitions of InSe to enhance its optical emissions. The modelling results suggest that, without the excitation of transition B', a strong optical emission enhancement up to hundreds of times can be obtained with incident light at an angle of less than 70° to the InSe layers. However, the enhancement will drop by several times as long as transition B' is excited by the incident light. These results provide useful references for the modulation of luminescent properties of InSe films toward flexible optoelectronic device applications.

2 Electronic structures and optical transitions

In order to understand the optical transitions involved in the optical emission enhancing process, we first investigate the electronic structure of few-layers InSe. Figures 1(a) and (b) show the orbitals projected electronic band structure of ML and 3-layer InSe, respectively. We can see that In-s orbitals dominate the CB edge, and Se-p_z orbitals dominate the VB edge. In the ML InSe, the second-highest VB becomes dominated by Se-p_{xy} orbitals. Because of spin-orbit coupling (SOC) effect, the VB edge is mixed with small amount of Se-p_{xy} orbital components as well. With the increase of thickness, there will be subbands emerging between the VB edge and the Se-p_{xy} orbitals dominated deeper VB. At Γ point, the first independent VB subband emerges in 3-layer InSe. These VB subbands are dominated by Se-p_z orbitals as well, but mixed with more Se-p_{xy} orbitals component than the VB edge, because they are more closed to the Se-p_{xy} orbitals dominated deeper VB and more affected by the SOC effect. We demonstrate this assumption by examining the ratio between the Se-p_z orbitals component and Se-p_{xy} orbitals component of VB edge and the second-highest VB of 1–9 layers InSe, as shown in Figure 1(c). The ratio between the Se-p_z orbitals component and Se-p_{xy} orbitals of the second-highest VB is always lower than the VB edge, demonstrating that it always contains more Se-p_{xy} orbitals components than the VB edge.

Thus, we proposed that, transition B', the optical transition between the second-highest VB and the

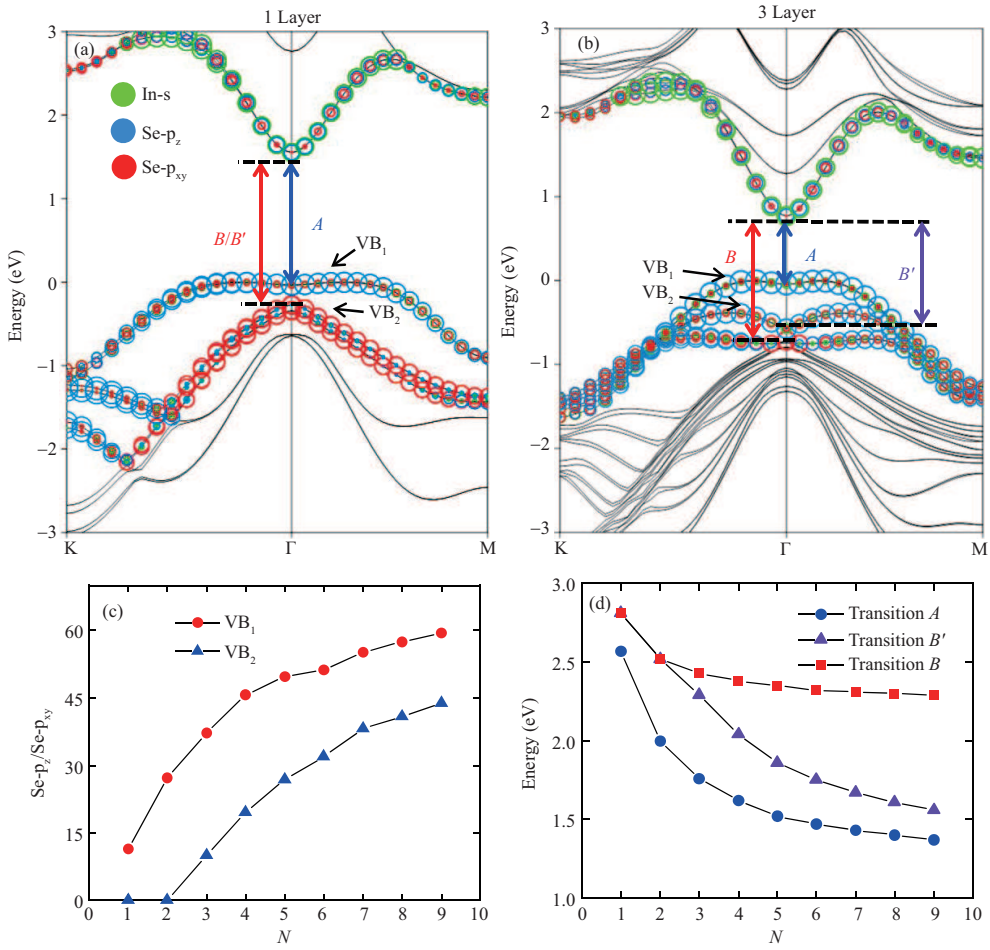

Figure 1 (Color online) Electronic structures and optical transitions of few-layers InSe. Projected band structure of (a) ML and (b) 3-layer InSe, with In-s orbital, Se-p_z orbital and Se-p_{xy} orbital indicated by green blue and red circles, respectively. (c) The ratio between the Se-p_z orbitals components and Se-p_{xy} orbitals components of VB edge and second-highest VB of 1–9 layers InSe. (d) The scissor corrected energies of transitions A, B', and B of 1–9 layers InSe.

bottom of CB, is also important while exploiting the anisotropy of optical transitions of InSe. Because the second-highest VB always contains more Se-p_{xy} orbital than VB edge, transition B' is more allowed for light polarized along the in-plane directions than transition A. The excitation of transition B' will increase the coupling to the in-plane polarized light and, by the same time, the coupling to the out-of-plane polarized light is not affected. Thus, the anisotropy of optical emissions, i.e., the emission enhancement along non-vertical directions, will be reduced. This assumption has been demonstrated in a recent experimental work [37] in which photoluminescence excitation (PLE) measurements were applied to detect the subbands structure of 5-layer and 7-layer InSe. The PLE results (excited by in-plane polarized light) clearly show that the excitation of transition B' will increase the optical emission for in-plane polarized light. The scissor corrected (see Section 6) energies of transitions A, B', and B of 1–9 layers InSe are shown in Figure 1(d). Transition B' and transition B are the same one in ML and 2-layer because there is no subband between the VB edge and the deeper VB dominated by Se-p_{xy} orbitals at Γ point in their electronic band structures.

3 Modelling the optical emission enhancement

To explore the origin and controlling method of the optical emission enhancement in bent regions of InSe thin film, we develop an analytical model of the PL process in bent and flat regions of InSe film to quantitatively simulate the enhancement. First, we define the component of the absorption coefficient that could effectively couple to the incident light as α^{eff}, i.e., the component of the absorption coefficient that projected in the polarization direction of the incident light. The difference in α^{eff} is the main reason

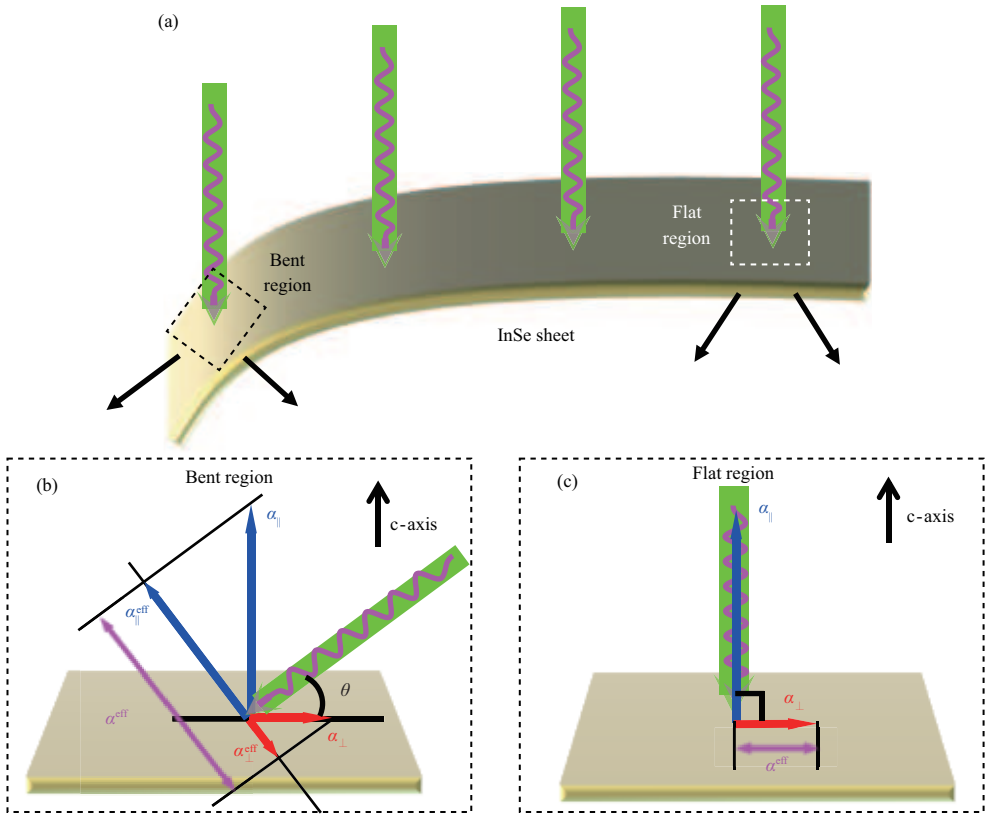

Figure 2 (Color online) (a) Scheme of the geometrical modified InSe sheet with bent and flat regions. Scheme of effective absorption coefficient in (b) bent region and (c) flat region.

for the different optical emission intensities in bent and flat regions. Figure 2(b) shows the representation of bent region of InSe film. We use $\alpha_{||}$ to represent the absorption coefficient for light polarized along out-of-plane direction ($\boldsymbol{E}\|\boldsymbol{c}$), and use $\alpha_{\perp}$ to represent the absorption coefficient for light polarized along the in-plane directions ($\boldsymbol{E}\perp\boldsymbol{c}$). For incident light at an angle θ to the InSe plane, we have $\alpha_{||}^{\rm eff}(\theta) = \cos\theta\alpha_{||}$ and $\alpha_{\perp}^{\rm eff}(\theta) = \sin\theta\alpha_{\perp}$. Thus, the total $\alpha^{\rm eff}(\theta)$ could be expressed as

$$\alpha^{\rm eff}(\theta) = \alpha_{||}^{\rm eff}(\theta) + \alpha_{\perp}^{\rm eff}(\theta) = \cos\theta\alpha_{||} + \sin\theta\alpha_{\perp}. \tag{1}$$

The incident light is perpendicular to the InSe plane in the flat region, i.e., $\theta = 90°$, thus the effective absorption coefficient in flat region to be $\alpha_{\theta=90°}^{\rm eff} = \alpha_{\perp}$, as shown in Figure 2(c).

To quantitatively simulate the optical emission enhancement, we consider a simplified model of the PL process. We assume that the probability that a photon with energy $E_{\rm exc}$ is absorbed by InSe is $P_{\rm abs}(E_{\rm exc})$; the probability that the photogenerated hot carriers relax to the band edge states is $P_{\rm rel}(E_{\rm exc}, E_{\rm g})$; the probability that photons of energy are emitted is $P_{\rm em}(E_{\rm g})$. Then, the PL intensity $I_{\rm PL}$ excited by excitation light with photon energy $E_{\rm exc}$ and intensity $I_{\rm ex}$ can be written as

$$I_{\rm PL}(E_{\rm exc}, E_{\rm g}, I_{\rm ex}) = P_{\rm abs}(E_{\rm exc}) \times P_{\rm rel}(E_{\rm exc}, E_{\rm g}) \times P_{\rm em}(E_{\rm g}) \times I_{\rm ex}. \tag{2}$$

Thus, the optical emission enhancement from bent region compared to flat region could be represented as

$$\text{Enhancement} = \frac{I_{\rm PL}(E_{\rm exc}, E_{\rm g}, I_{\rm ex})_{\rm bent}}{I_{\rm PL}(E_{\rm exc}, E_{\rm g}, I_{\rm ex})_{\rm flat}} = \frac{P_{\rm abs}(E_{\rm exc})_{\rm bent}}{P_{\rm abs}(E_{\rm exc})_{\rm flat}} \times \frac{P_{\rm rel}(E_{\rm exc}, E_{\rm g})_{\rm bent}}{P_{\rm rel}(E_{\rm exc}, E_{\rm g})_{\rm flat}} \times \frac{P_{\rm em}(E_{\rm g})_{\rm bent}}{P_{\rm em}(E_{\rm g})_{\rm flat}} \times \frac{I_{\rm ex}}{I_{\rm ex}}. \tag{3}$$

The $P_{\rm abs}(E_{\rm exc})$ and $P_{\rm em}(E_{\rm g})$ are proportional to the absorption coefficient $\alpha(E_{\rm exc})$ and $\alpha(E_{\rm g})$, and thus we can get

$$\frac{P_{\rm abs}(E_{\rm exc})_{\rm bent}}{P_{\rm abs}(E_{\rm exc})_{\rm flat}} = \frac{\alpha(E_{\rm exc})_{\rm bent}}{\alpha(E_{\rm exc})_{\rm flat}} = \frac{\alpha^{\rm eff}(E_{\rm exc}, \theta)}{\alpha_{\theta=90°}^{\rm eff}(E_{\rm exc})} = \cos\theta\frac{\alpha_{||}(E_{\rm exc})}{\alpha_{\perp}(E_{\rm exc})} + \sin\theta, \tag{4}$$

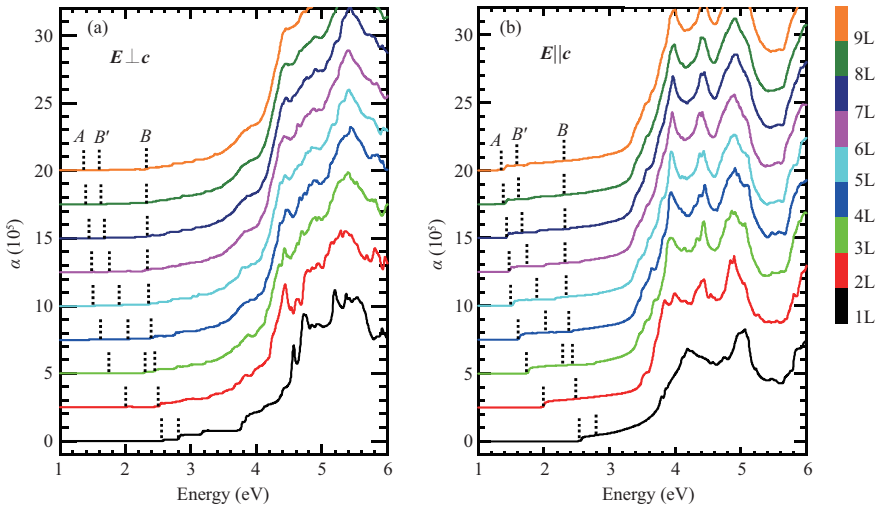

Figure 3 (Color online) Absorption coefficients for electric field dipole E (a) perpendicular and (b) parallel to the c-axis. Results of 1–9 layers InSe are represented by curves with different colors, respectively. The energies of transitions A, B', and B of different layers are indicated by short dash lines on each curve.

and

$$\frac{P_{\rm em}(E_{\rm g})_{\rm bent}}{P_{\rm em}(E_{\rm g})_{\rm flat}} = \frac{\alpha(E_{\rm g})_{\rm bent}}{\alpha(E_{\rm g})_{\rm flat}} = \frac{\alpha^{\rm eff}(E_{\rm g},\theta)}{\alpha^{\rm eff}_{\theta=90^\circ}(E_{\rm g})} = \cos\theta\frac{\alpha_{||}(E_{\rm g})}{\alpha_{\perp}(E_{\rm g})} + \sin\theta. \tag{5}$$

For two excitation light with the same photon energy and intensity, $P_{\rm rel}(E_{\rm exc},E_{\rm g})$ and $I_{\rm ex}(E_{\rm exc})$ remains unchanged. Which means that $\frac{P_{\rm rel}(E_{\rm exc},E_{\rm g})_{\rm bent}}{P_{\rm rel}(E_{\rm exc},E_{\rm g})_{\rm flat}} = \frac{I_{\rm ex}}{I_{\rm ex}} = 1$. Thus, the optical emission enhancement from bent region compared to flat region could be finally represented as

$$\text{Enhancement} = \left(\cos\theta\frac{\alpha_{||}(E_{\rm exc})}{\alpha_{\perp}(E_{\rm exc})} + \sin\theta\right) \times \left(\cos\theta\frac{\alpha_{||}(E_{\rm g})}{\alpha_{\perp}(E_{\rm g})} + \sin\theta\right), \tag{6}$$

which is a function of $E_{\rm exc}$ and θ for a InSe film with given thickness.

4 Absorption coefficients and modelling results

To get the numerical solution of the optical emission enhancement expression, we calculate the absorption coefficients of 1–9 layers InSe. Figures 3(a) and (b) show the scissor corrected energy dependent absorption coefficients $\alpha_{\perp}$ and $\alpha_{||}$. For $\alpha_{\perp}$, there are only small values of α at the energy of transition A (optical band gap energy), and it starts to increase after the energy of transition B', which can be seen more clearly in Figure 4(b). For $\alpha_{||}$, the value of α is markedly enhanced compared to $\alpha_{\perp}$ from the energy of transition A to nearly 3 eV, which clearly shows the large anisotropy of optical transitions of InSe.

Then we examine the dependence of $\alpha_{||}/\alpha_{\perp}$ on energy. The $\alpha_{||}/\alpha_{\perp}$ results of 1–3 and 9 layers InSe are presented in Figure 4(a). The $\alpha_{||}$ and $\alpha_{\perp}$ within the same energy range of the corresponding materials are shown in Figure 4(b). From Figure 4(a), we can see that $\alpha_{||}/\alpha_{\perp}$ always get the maximum value between energy range from the energy of transition A to the energy of transition B', consisting of the analysis in Section 2.

After obtaining the dependence of $\alpha_{||}/\alpha_{\perp}$ on energy, we can determine the specific distribution and maximum value of the optical emission enhancement. Figure 5 shows the colored contour maps of the optical emission enhancement of 1–9 layers InSe, as a function of $E_{\rm exc}$ and θ. The results show that the maximum enhancement up to hundreds of times can be achieved from the bent region of few layers InSe, with a small θ, 16.05° for ML InSe, less than 5.1° for InSe of other thickness, and an $E_{\rm exc}$ in the energy range between transition A and B'. When $E_{\rm exc}$ is lower than the energy of transition B', there is always strong enhancement as long as $\theta < 70°$. Once $E_{\rm exc}$ is larger than the energy of transition B', i.e., once transition B' is excited, the enhancement will rapidly drop by a factor of several times, because

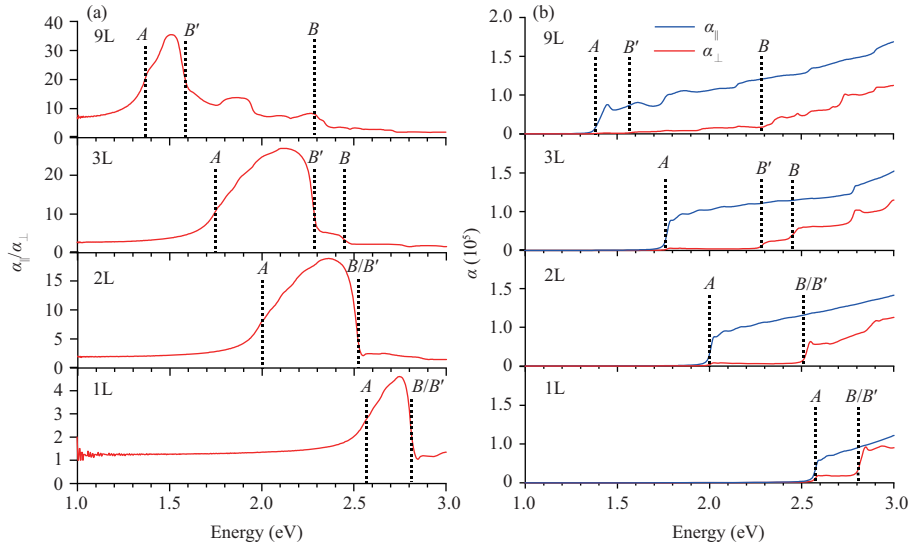

Figure 4 (Color online) (a) The ratio of $\alpha_{||}/\alpha_{\perp}$ of 1–3 and 9 layers InSe with respect to energy. (b) The absorption coefficient $\alpha_{||}$ and $\alpha_{\perp}$ of 1–3 and 9 layers InSe. The energies of optical transitions A, B' and B are indicated by dash lines in each graph.

the emission from flat region grows owing to the excitation of transition B' while the emission from bent region is not affected.

5 Conclusion

In conclusion, we explored the mechanism of the optical emission enhancement from the bent regions of InSe thin film compared to flat regions by modelling the photoluminescence processes in bent and flat regions of the InSe thin film. Our model shows that the shorter-wavelength interband transition, labelled as transition B', between the second-highest valence band and the bottom of conduction band, significantly influences the emission enhancement. The modelling results robustly describe the dependence of optical emission enhancement in the bent InSe thin films on thickness, incident light orientation, and excitation photon energy. We found that strong enhancement up to hundreds of times can be obtained by applying an incident light at an angle less than 70° to the InSe layers, with excitation photon energy lower than the energy of transition B'. These results provide useful references for modulating luminescent properties of InSe films toward flexible optoelectronic device applications.

6 Methods

The first-principles calculations are based on density functional theory (DFT) using the plane-wave pseudopotential method as implemented in the Vienna Ab Initio Simulation Package [38,39]. Generalized gradient approximation formulated by Perdew, Burke, and Ernzerhof was used as exchange-correlation functional [40]. Projected augmented wave pseudopotentials with 5s25p1(In), 4s24p4(Se) treated as valence electrons were used to describe the electron-ion interactions. Plane-wave energy cutoff of 450 eV was used for all calculations, and k-points grid spacing was set to $2\pi \times 0.03\text{Å}^{-1}$ for Brillouin zone integration. To simulate the atomic thin InSe layers, a vacuum layer space with thickness greater than 15 was employed to separate the InSe layer from their periodic images. The interlayer distance of multilayer InSe was optimized by minimizing the total energy including the vdW interaction described by the optB86b-vdW functional [41]. The residual forces on atoms were converged to below 0.05 eVÅ^{-1} for all structure optimization calculations. To obtain an accurate description of optical properties near the bandgap energy, refined Brillouin zone sampling was used for the optical property calculations. Γ-centered k-points mesh with an extremely high density of 48×48×1, 40×40×1, 36×36×1 and 32×32×1 were used for 1–5, 6–7, 8 and 9 layers, respectively. The absorption coefficients are calculated by equation $\alpha(\omega) = \sqrt{2}\omega[\frac{\sqrt{\varepsilon_1(\omega)^2+\varepsilon_2(\omega)^2}-\varepsilon_1(\omega)}{2}]^{\frac{1}{2}}$, where $\varepsilon_1(\omega)$ and $\varepsilon_2(\omega)$ are the real and imaginary parts of the frequency-dependent complex dielectric function. To offset the well-known bandgap energy underestimation issue of

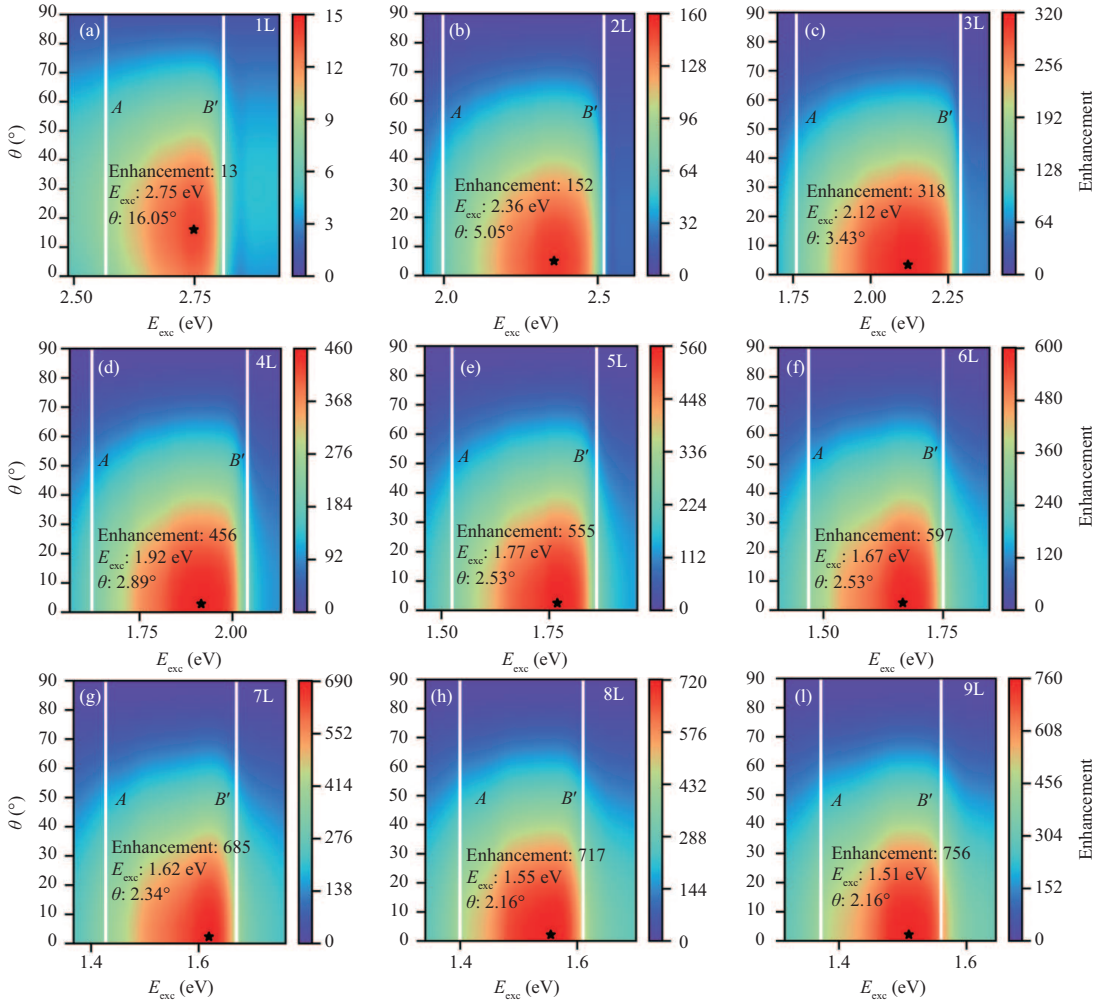

Figure 5 (Color online) The optical emission enhancement model results. (a)–(l) The colored contour maps of the optical emission enhancement of 1–9 layers InSe, respectively, as a function of the photon energy of the incident light and its angle with the InSe plane. The color represents the value of the enhancement. The maximum enhancement with its corresponding $E_{\rm exc}$ and θ is marked out with a star in each graph. The energies of transitions A and B' are indicated by white lines in each graph.

DFT calculation, a scissor operator with the same magnitude of the bandgap difference between the values calculated by DFT and obtained from the experimental measurement was used. Spin-orbital coupling was included in all calculations. It introduces a fundamental change to the orbital compositions of the electronic states near the band edge, which affects the optical properties.

Acknowledgements This work was supported by National Natural Science Foundation of China (Grants Nos. 61722403, 11674121) and Jilin Province Science and Technology Development Program (Grants No. 20190201016JC). Calculations were performed in part at the High-performance Computing Center of Jilin University.

References

1 Wang J, Han J, Chen X, et al. Design strategies for two-dimensional material photodetectors to enhance device performance. Infomat, 2019, 1: 33–53
2 Zhang X, Kawai H, Yang J, et al. Detecting MoS2 and MoSe2 with optical contrast simulation. Prog Nat Sci-Mater Int, 2019, 29: 667–671
3 Wang Z, Zhao D, Yu S, et al. First-principles investigation of structural and electronic properties of oxygen adsorbing phosphorene. Prog Nat Sci-Mater Int, 2019, 29: 316–321
4 Tao L, Chen Z, Li Z, et al. Enhancing light-matter interaction in 2D materials by optical micro/nano architectures for high-performance optoelectronic devices. Infomat, 2021, 3: 36–60
5 Tang H, Hu Q, Zheng M, et al. MXene-2D layered electrode materials for energy storage. Prog Nat Sci-Mater Int, 2018, 28: 133–147
6 Neto A H C, Guinea F, Peres N M R, et al. The electronic properties of graphene. Rev Mod Phys, 2009, 81: 109–162
7 Mak K F, Sfeir M Y, Misewich J A, et al. The evolution of electronic structure in few-layer graphene revealed by optical spectroscopy. Proc Natl Acad Sci USA, 2010, 107: 14999–15004
8 Zhao X G, Shi Z, Wang X, et al. Band structure engineering through van der Waals heterostructing superlattices of twodimensional transition metal dichalcogenides. Infomat, 2020, 84: inf2.12155

9 Liu Z, Na G, Tian F, et al. Computational functionality-driven design of semiconductors for optoelectronic applications. Infomat, 2020, 2: 879–904
10 Tong X, Zhan X, Rawach D, et al. Low-dimensional catalysts for oxygen reduction reaction. Prog Nat Sci-Mater Int, 2020, 30: 787–795
11 Wang T, Shi X Y, Wang J, et al. Nonlinear photoresponse of metallic graphene-like VSe2 ultrathin nanosheets for pulse laser generation. Sci China Inf Sci, 2019, 62: 220406
12 Wu B M, Wang X D, Tang H W, et al. A study on ionic gated MoS2 phototransistors. Sci China Inf Sci, 2019, 62: 220405
13 Mudd G W, Svatek S A, Ren T, et al. Tuning the bandgap of exfoliated InSe nanosheets by quantum confinement. Adv Mater, 2013, 25: 5714–5718
14 Brotons-Gisbert M, Andres-Penares D, Suh J, et al. Nanotexturing to enhance photoluminescent response of atomically thin indium selenide with highly tunable band gap. Nano Lett, 2016, 16: 3221–3229
15 Bandurin D A, Tyurnina A V, Yu G L, et al. High electron mobility, quantum Hall effect and anomalous optical response in atomically thin InSe. Nat Nanotech, 2017, 12: 223–227
16 Mazumder D, Xie J, Kudrynskyi Z R, et al. Enhanced optical emission from 2D InSe bent onto Si-Pillars. Adv Opt Mater, 2020, 8: 2000828
17 Tamalampudi S R, Lu Y Y, Ulaganathan R K, et al. High performance and bendable few-layered InSe photodetectors with broad spectral response. Nano Lett, 2014, 14: 2800–2806
18 Sun Y, Li Y, Li T, et al. New polymorphs of 2D indium selenide with enhanced electronic properties. Adv Funct Mater, 2020, 30: 2001920
19 Song C, Fan F, Xuan N, et al. Largely tunable band structures of few-layer InSe by uniaxial strain. ACS Appl Mater Interfaces, 2018, 10: 3994–4000
20 Song C, Huang S, Wang C, et al. The optical properties of few-layer InSe. J Appl Phys, 2020, 128: 060901
21 Zhao Q, Frisenda R, Wang T, et al. InSe: a two-dimensional semiconductor with superior flexibility. Nanoscale, 2019, 11: 9845–9850
22 Arora H, Erbe A. Recent progress in contact, mobility, and encapsulation engineering of InSe and GaSe. Infomat, 2020, 1: inf2.12160
23 Zhao C, Gao W, Jiang Q. CO adsorption on metal doped 2D InSe: mechanism and application. Prog Nat Sci-Mater Int, 2019, 29: 305–309
24 Yang H, Xiao M Q, Cui Y, et al. Nonvolatile memristor based on heterostructure of 2D room-temperature ferroelectric α-In_2Se_3 and WSe_2. Sci China Inf Sci, 2019, 62: 220404
25 Sun Y, Luo S, Zhao X-G, et al. InSe: a two-dimensional material with strong interlayer coupling. Nanoscale, 2018, 10: 7991–7998
26 Shi Z, Wang X, Sun Y, et al. Interlayer coupling in two-dimensional semiconductor materials. Semicond Sci Technol, 2018, 33: 093001
27 Zhang L, Zunger A. Evolution of electronic structure as a function of layer thickness in group-VIB transition metal dichalcogenides: emergence of localization prototypes. Nano Lett, 2015, 15: 949–957
28 Zeng J, He X, Liang S-J, et al. Experimental identification of critical condition for drastically enhancing thermoelectric power factor of two-dimensional layered materials. Nano Lett, 2018, 18: 7538–7545
29 Kang J, Zhang L, Wei S-H. A unified understanding of the thickness-dependent bandgap transition in hexagonal two-dimensional semiconductors. J Phys Chem Lett, 2016, 7: 597–602
30 Camassel J, Merle P, Mathieu H, et al. Excitonic absorption edge of indium selenide. Phys Rev B, 1978, 17: 4718–4725
31 Brotons-Gisbert M, Proux R, Picard R, et al. Out-of-plane orientation of luminescent excitons in two-dimensional indium selenide. Nat Commun, 2019, 10: 3913
32 Li Y, Wang T, Wang H, et al. Enhanced light emission from the ridge of two-dimensional InSe flakes. Nano Lett, 2018, 18: 5078–5084
33 Magorrian S J, Zólyomi V, Fal'ko V I. Electronic and optical properties of two-dimensional InSe from a DFT-parametrized tight-binding model. Phys Rev B, 2016, 94: 245431
34 Hamer M J, Zultak J, Tyurnina A V, et al. Indirect to direct gap crossover in two-dimensional inse revealed by angle-resolved photoemission spectroscopy. ACS Nano, 2019, 13: 2136–2142
35 Li Y, Wang T, Wu M, et al. Ultrasensitive tunability of the direct bandgap of 2D InSe flakes via strain engineering. 2D Mater, 2018, 5: 021002
36 Ubrig N, Ponomarev E, Zultak J, et al. Design of van der Waals interfaces for broad-spectrum optoelectronics. Nat Mater, 2020, 19: 299–304
37 Zultak J, Magorrian S J, Koperski M, et al. Ultra-thin van der Waals crystals as semiconductor quantum wells. Nat Commun, 2020, 11: 125
38 Kresse G, Furthmüller J. Efficient iterative schemes for ab initio total-energy calculations using a plane-wave basis set. Phys Rev B, 1996, 54: 11169–11186
39 Kresse G, Furthmüller J. Efficiency of ab-initio total energy calculations for metals and semiconductors using a plane-wave basis set. Comput Mater Sci, 1996, 6: 15–50
40 Perdew J P, Burke K, Ernzerhof M. Generalized gradient approximation made simple. Phys Rev Lett, 1996, 77: 3865–3868
41 Klimeš J, Bowler D R, Michaelides A. Chemical accuracy for the van der Waals density functional. J Phys Condens Matter, 2010, 22: 022201